Research Article | Vol. 30, No. 26 / 19 Dec 2022 / Optics Express 47235
Optics EXPRESS

Laser cooling in Yb:KY_3F_{10}: a comparison with Yb:YLF

STEFAN PÜSCHEL, FELIX MAUERHOFF, CHRISTIAN KRÄNKEL, AND HIROKI TANAKA*

Leibniz-Institut für Kristallzüchtung (IKZ), Max-Born-Str. 2, 12489 Berlin, Germany
**hiroki.tanaka@ikz-berlin.de*

Abstract: Laser cooling by anti-Stokes fluorescence is a technology to realize all-solid-state optical cryocoolers. We grew Yb^{3+}-doped KY_3F_{10} (Yb:KYF) crystals as novel laser cooling media and compare their cooling performance to Yb^{3+}-doped $LiYF_4$ (Yb:YLF) crystals also grown in our institute. We present temperature-dependent absorption and emission cross sections as well as the fluorescence lifetime of Yb:KYF, and calculate its material figure-of-merit for laser cooling. Yb:KYF exhibits a higher figure-of-merit than Yb:YLF at temperatures below 200 K. This is because, in contrast to Yb:YLF, the excitation transition from the second-highest Stark level of the ground state is best-suited for cryogenic cooling in Yb:KYF. Thus, it has the potential to achieve unprecedentedly low temperatures below the boiling point of liquid nitrogen. In this work, we observe the first laser cooling of Yb:KYF, and obtain a background absorption coefficient of $\sim 10^{-4}$ cm^{-1}, which is among the lowest ever reported for Yb^{3+}-doped fluoride crystals. A simple model calculation predicts that our Yb:KYF and Yb:YLF crystals can potentially be cooled down to ≈100 K in a high-power cooling setup. Our Yb:KYF crystals still leave room for further improvement through the optimization of the growth process and the use of purer raw materials.

1. Introduction

Cooling of solids by anti-Stokes fluorescence [1,2] has gathered great attention within the last decade. This is because cryogenic cooling is indispensable in many fields of science, *e.g.*, to reduce the noise level of infrared and gamma-ray detectors [3,4]. In contrast to cryocoolers based on liquefied gases, anti-Stokes fluorescence cooling is intrinsically compact and vibration-free, which is relevant for example in space-borne applications [5]. The concept of anti-Stokes fluorescence cooling was introduced nearly 100 years ago: If the fluorescence photons have on average higher energy than the excitation photons, the fluorescence removes energy from the material, and hence reduces its temperature by annihilating phonons in each anti-Stokes cycle [6]. First cooling was demonstrated in an Yb^{3+}-doped fluorozirconate glass in 1995 [7], and nowadays laser cooling to cryogenic temperatures, commonly defined to be below 123 K, is routinely achieved mainly using Yb^{3+}-doped $LiYF_4$ (Yb:YLF) as the cooling medium [8–12]. In particular Yb-doped fluoride crystals and glasses have proven to be well-suited cooling materials mainly for two reasons: First, their low crystal field strength, resulting in a small Stark splitting of the energy multiplets, causes a strong overlap between emission and absorption spectra even at low temperatures. This enhances the absorption of photons with energies below the mean fluorescence energy. Second, the large energetic gap between the ground and excited state of Yb^{3+} suppresses non-radiative decay by multi-phonon relaxation, yielding high fluorescence quantum efficiencies close to unity. Meanwhile, several host crystals have been tested for laser cooling, including $LiLuF_4$ [8,13], KYF_4 [14], CaF_2 [15], SrF_2 [15] and BaY_2F_8 [16,17], but for most of them, except Yb:$LiLuF_4$, the cooling potential is not yet fully explored. Therefore, Yb:YLF is still a state-of-the-art material for laser cooling. The current record cooling temperature is 87 K [18,19], which is only 10 K above the boiling point of liquid nitrogen (LN) at 77 K.

#472633 https://doi.org/10.1364/OE.472633
Journal © 2022 Received 9 Aug 2022; revised 20 Oct 2022; accepted 14 Nov 2022; published 13 Dec 2022

Optics EXPRESS

Here, we investigate the potential of the cubic KY_3F_{10} crystal doped with Yb^{3+} (Yb:KYF) as a laser cooling medium in comparison with Yb:YLF. We describe the Czochralski growth of Yb:KYF and Yb:YLF crystals and present temperature-dependent absorption and emission cross sections, as well as the temperature-dependent fluorescence lifetime of Yb:KYF. These data enable to compare Yb:KYF with Yb:YLF with respect to its potential for laser cooling. We find that Yb:KYF exhibits the potential for higher cooling efficiencies than Yb:YLF at temperatures below 200 K, and the laser cooling figure-of-merit for Yb:KYF becomes even eight times larger than that of Yb:YLF at 77 K. We demonstrate the first laser cooling of Yb:KYF and present the results of laser-induced thermal modulation spectroscopy (LITMoS) tests for a systematic comparison with Yb:YLF crystals. Our calculations predict that both Yb:KYF and Yb:YLF grown from raw materials of 99.99% – 99.999% (*i.e.*, 4N – 5N) purity grade can be cooled down to ≈100 K, and even lower temperatures are achievable for Yb:KYF with only minor improvements of the crystal purity. Thus, we propose Yb:KYF as a promising laser cooling medium to reach the LN boiling point.

2. Crystal growth

We grew two Yb:KYF crystals by the Czochralski method. The raw materials were KF powder (Fox Chemicals GmbH) with 4N purity, YbF_3 powder (AC Materials, Inc.) with 5N purity, and two different YF_3 powders. For the first crystal (Yb:KYF-1) we used YF_3 (Alfa Aesar) with 4N purity, and for the second crystal (Yb:KYF-2) we used YF_3 (Projector GmbH) with 99.9995% (5N5) purity. In all growth experiments presented here, prior to the growth, the starting powders were fluorinated by purging them with a mixture of Ar and HF gas for 4 h at 800°C to reduce the amount of trace oxygen, oxyfluoride, and moisture [20]. Since KYF is congruently melting, both crystals were grown from a stoichiometric melt with a target Yb doping level of 3% corresponding to a composition of $K(Y_{0.97}Yb_{0.03})_3F_{10}$. For Yb:KYF-1 we used a graphite crucible coated with pyrolytic carbon (SGL Carbon SE), while for Yb:KYF-2 a glassy carbon crucible (HTW Hochtemperatur-Werkstoffe GmbH) was used. Both crystals were seeded with an undoped KYF crystal and grown along the crystallographic [100]-direction in a growth atmosphere of Ar mixed with 5 vol.% CF_4 to prevent the formation of Yb^{2+} [21]. The size of both as-grown boules was 20 mm in diameter and ≈80 mm in length. The crystals contained light-scattering centers visualized by an irradiation of a HeNe laser, and their bottom part exhibited whitish inclusions. These are possibly due to residual oxides in the raw materials [22], in particular in the hygroscopic KF. The Yb doping level in the grown crystals was determined to be 2.7 ± 0.1% using an X-ray fluorescence (XRF) spectrometer (Bruker, M4 TORNADO). The inclusions in the bottom part did not show any detectable change in the X-ray fluorescence signal, so they could be composed of elements lighter than sodium, which is the lightest element detectable by the spectrometer, *e.g.* oxygen containing phases.

Besides the Yb:KYF crystals, we also grew three Yb:YLF crystals by the Czochralski method. These were grown from different raw materials of various purity. The first and second crystals (Yb:YLF-1 and Yb:YLF-2) were grown from identical raw materials, 4N purity LiF (Auer Remy GmbH) and 5N5 purity YF_3 (Projector GmbH). Yb:YLF-1 was grown from a pyrolytic-carbon-coated graphite crucible (SGL Carbon SE) along the [001]-direction. Instabilities during its growth process caused by dirt on the melt surface, considered to be organic residue, led to many small-angle grain boundaries as well as scattering centers. Yb:YLF-2 grown from a platinum crucible along the [110]-direction showed no scattering centers. The third crystal (Yb:YLF-3) was grown from LiF and YF_3 converted respectively from 5N purity Li_2CO_3 (Acros Organics B.V.B.A.) and Y_2O_3 (Lehmann & Voss & Co KG) by the fluorination using HF gas. It was grown from a platinum crucible and did not show any scattering centers. For all the Yb:YLF crystals, the powders were weighed for a target Yb doping level of 5%. To avoid the precipitation of YF_3 due to the peritectic reaction reported for melts containing more than 49 mol.% YF_3 [23],

Optics EXPRESS

these crystals were grown from a non-stoichiometric composition with 2 mol.% excess of LiF. The Yb doping level in the grown crystals was determined to be between 4.5 and 4.8% by XRF spectroscopy.

The parameters and conditions of the growth of the Yb:KYF and Yb:YLF crystals are summarized in Tab. 1. We chose the lower doping level of 3% for Yb:KYF ($4.7\times10^{20}\,cm^{-3}$) rather than 5% as in Yb:YLF ($7.0\times10^{20}\,cm^{-3}$) because we anticipated a stronger influence of fluorescence reabsorption in Yb:KYF than in Yb:YLF from the spectroscopic data in the literature [24]. Note that we used the identical YbF_3 (AC Materials, Inc., 5N purity) for all five crystals, so possible variations of the foreign rare-earth impurity level should arise from the purity of the YF_3 starting materials.

Table 1. Growth conditions and parameters of Yb:KYF and Yb:YLF crystals.

Crystal	KF/LiF purity	YF_3 purity	YbF_3 purity	Nominal Yb doping level [%]	Growth direction	Growth speed [mm/h]	Crucible material	Growth atmosphere
Yb:KYF-1	4N	4N	5N	3	[100]	1.0–1.5	graphite	Ar + CF_4 (5 vol.%)
Yb:KYF-2	4N	5N5	5N	3	[100]	1.0–1.2	glassy carbon	Ar + CF_4 (5 vol.%)
Yb:YLF-1	4N	5N5	5N	5	[001]	1.0	graphite	Ar + CF_4 (5 vol.%)
Yb:YLF-2	4N	5N5	5N	5	[110]	1.0	platinum	Ar + CF_4 (5 vol.%)
Yb:YLF-3	5N[a]	5N[b]	5N	5	[110]	1.0	platinum	Ar + CF_4 (5 vol.%)

[a]Converted from 5N Li_2CO_3.
[b]Converted from 5N Y_2O_3.

3. Spectroscopic characterization of Yb:KYF

In contrast to the tetragonal YLF, KYF is a cubic crystal. It has been used successfully as a laser host material for trivalent rare-earth ions such as Pr^{3+} [25], Nd^{3+} [26,27], or Tm^{3+} [28]. KYF crystallizes in a superstructure of fluorite with eight formula units. The structure can be described as an undulating combination of $[KY_3F_8]^{2+}$ and $[KY_3F_{12}]^{2-}$ clusters [29]. In KYF, the coordination polyhedra of the Y^{3+}-sites, substituted by rare-earth ions, are antiprisms with local symmetry axes parallel to the crystallographic <100>-axes. As a result, despite the cubic structure, rare-earth ions doped in KYF may differently interact with linearly polarized light depending on the symmetry axes of the substitution sites. This causes polarization effects in the fluorescence spectrum of Pr:KYF [30], but we did not observe this effect in a <100>-cut Yb:KYF crystal. The maximum phonon energy of 495 cm^{-1} of KYF [31] is slightly higher than that of YLF (450 cm^{-1} [32]), but still sufficiently low to fully inhibit multi-phonon relaxation bridging the ≈10,000 cm^{-1} energy gap between the excited and the ground states of Yb^{3+}. KYF may also be a useful crystalline host for laser cooling based on Tm^{3+} or Ho^{3+}, in which the energetic position of the first excited states are lower than in Yb^{3+}, according to the internal quantum efficiency criterion for laser cooling (the energy separation between the ground- and first excited-states should be more than eight times larger than the maximum phonon energy) [33].

Similar to the spectroscopy of Yb:YLF described in [34], we performed temperature-dependent transmission and fluorescence spectroscopy as well as fluorescence lifetime measurements for Yb:KYF. We investigated our samples prepared from the crystal Yb:KYF-1 in a temperature range between 15 K and 300 K using a closed-cycle helium cryostat. We used a high-resolution monochromator (HORIBA, M1000) with a photomultiplier tube (Hamamatsu, R5108) as a detector. For transmission spectroscopy, a tungsten-halogen lamp was utilized as a broadband light source. To avoid reabsorption effects affecting the detected fluorescence spectral shape, a 200 µm thin sample was used in the corresponding experiments. Figure 1(a) shows the absorption

Optics EXPRESS

and emission cross section spectra of Yb:KYF at room temperature. The measured fluorescence intensity spectra were corrected for the sensitivity of the measurement setup. The emission cross section spectrum was calculated by the Füchtbauer-Ladenburg formula [35] using the experimentally determined radiative lifetime of 1.86 ms described below. The absorption cross section spectrum was calculated from the transmission spectrum by the Beer-Lambert law using the Yb concentration determined by XRF spectroscopy, and also calculated via the reciprocity relation [36] from the emission cross section spectrum. The agreement of the two absorption cross section spectra shown in Fig. 1(a) evidences that due to the use of a thin sample the measured fluorescence spectrum was unaffected by reabsorption, despite the large overlap of the absorption and emission spectra at room temperature. To resolve all features of the absorption spectrum at 15 K, the 200 µm thin sample was used for wavelengths above 960 nm and a thick sample of 12 mm was used to resolve the significantly weaker features at shorter wavelengths.

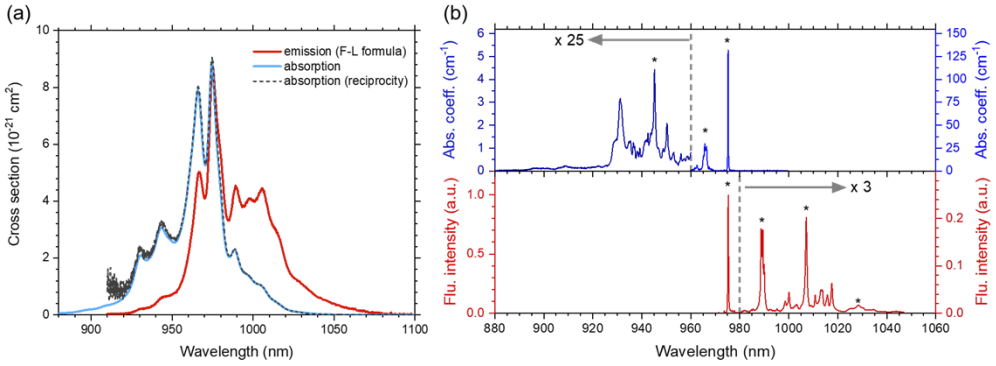

Fig. 1. (a) Absorption and emission cross section spectra of Yb:KYF at room temperature. The emission cross sections were calculated by the Füchtbauer-Ladenburg (F-L) formula. The absorption cross sections were obtained from the transmission spectrum with the Yb concentration determined by XRF spectroscopy and in addition calculated using the reciprocity relation from the emission cross section spectrum with a radiative lifetime of 1.86 ms (presented below). (b) Absorption coefficients and fluorescence spectra at 15 K. The assigned resonant transitions between Stark levels are marked by *. The other peaks are considered to be phonon replicas [24]. To resolve the weak features in the short (< 960 nm) wavelength part of the absorption, a different, 12 mm thick sample was used for this range. For better visibility, the y-axis is enhanced by a factor of 25 in this range. The fluorescence spectra were recorded with the same sample (200 µm) throughout the whole range, but for better visibility, the y-axis is enhanced by a factor of three for wavelengths > 980 nm.

From the spectra shown in Fig. 1(b) we determined the energetic positions of the ground- and excited-state Stark levels of Yb^{3+} in KYF. Figure 2(a) shows the resulting Stark energy level diagram. Our spectra are in good agreement with previous data [24,37] which, however, differently determined the position of the levels E4 and E7. We assign the peak around 1028 nm in Fig. 1(b) to the transition E5→E4 in agreement with [24]. This is consistent with the temperature-dependent emission cross sections presented below [cf. Figure 4(a)]. Among the three main absorption peaks at wavelengths shorter than 960 nm, the peak at 945.1 nm is assigned to the transition E1→E7 owing to its narrowest feature. Figure 2(b) shows the fractional occupancy of each Stark level calculated by the Boltzmann distribution function using the determined energetic position for a temperature range of 0–300 K. These graphs also show that the actual assignment of E4 and E7 has little influence on the partition functions required in the reciprocity method.

Optics EXPRESS

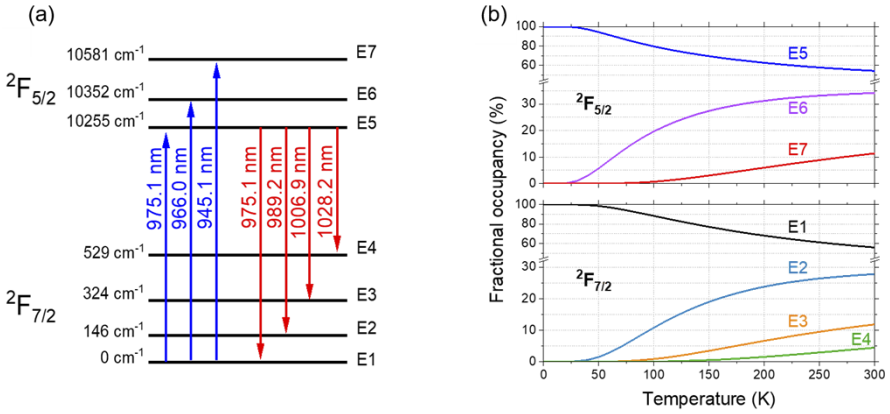

Fig. 2. (a) Energy diagram of Yb^{3+} in KY_3F_{10} with the Stark level positions and corresponding wavelengths of the resonant absorption and emission transitions. (b) Fractional occupancy of the ground-state ($^2F_{7/2}$) and excited-state ($^2F_{5/2}$) Stark levels as a function of temperature according to the Boltzmann distribution.

For a precise determination of the temperature-dependent emission cross sections, the knowledge of the temperature-dependent radiative lifetime is essential. To this end, we measured the fluorescence decay of a sample prepared from the crystal Yb:KYF-1 at various temperatures. To minimize the influence of radiation trapping on the measured fluorescence lifetime, the pinhole method [38] was applied for room temperature measurements where pinholes of different diameters are placed in front of the sample to vary the excited volume. Figure 3(a) shows the measured fluorescence lifetimes with respect to the pinhole diameter. A linear extrapolation to a 0-mm pinhole diameter yields the intrinsic fluorescence lifetime, free of radiation trapping, to be $\tau_{rad} = 1.86 \pm 0.07$ ms. This agrees with the previously reported value of 1.77 ms for Yb(0.5%):KYF [39] and the value of 1.87 ms proposed in [40]. For lower temperatures, we used the ≈200 µm thin sample which had been proven to effectively suppress reabsorption in the fluorescence measurements as illustrated in Fig. 1(a). Figure 3(b) shows the fluorescence lifetime of Yb:KYF versus temperature. The result of the pinhole method indicated as a red square symbol agrees with the value obtained with the thin sample (blue circles). Considering the decreasing influence of reabsorption with decreasing temperature, this indicates a successful suppression of radiation trapping in all temperature-dependent fluorescence lifetime measurements performed without using the pinhole method. We observed an increase of the fluorescence lifetime up to 3.2 ms with decreased temperatures down to 15 K. For Yb^{3+} ions in the trigonal host KYF_4, a similar trend was observed and attributed to a temperature-dependent energy transfer from Yb^{3+} to Er^{3+} and Ho^{3+} impurities which quench the lifetime of Yb^{3+} [41]. Such effect would be extremely detrimental for laser cooling. In contrast, we previously attributed the strong temperature dependence of the radiative lifetime to the population distribution of excited Yb^{3+} in the three upper Stark levels having individual radiative lifetimes in Yb:YLF [34]. A corresponding fit considering the fractional occupancies of the levels E5, E6, and E7 as seen in Fig. 2(b) yields individual lifetimes for the lower two Stark levels of the upper $^2F_{5/2}$ manifold of the Yb^{3+} ion (E5 and E6) of $\tau_{E5} = 3.2$ ms and $\tau_{E6} = 1.1$ ms. The small fractional occupancy of the highest level E7 leads to a significant fit-error for τ_{E7} which is thus roughly estimated to be longer than 4 ms; a more accurate determination would require further measurements at elevated temperatures.

With these lifetime data, we were able to determine the temperature-dependent cross sections of Yb:KYF as shown in Fig. 4. The emission cross section spectra in Fig. 4(a) were calculated by

Optics EXPRESS

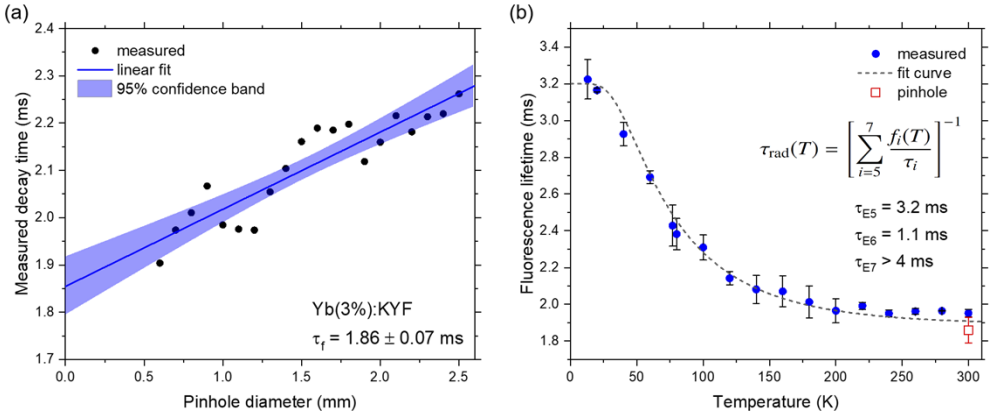

Fig. 3. (a) Fluorescence decay time of Yb(3%):KYF measured with a variety of pinhole diameters. (b) Temperature-dependent fluorescence lifetimes. The measured values are shown as blue circles. The value at room temperature determined by the pinhole method is shown as a red square. The dashed line is the result of a fitting with the equation shown in the graph, yielding the individual lifetimes of the upper Stark levels denoted in the graph, too.

the Füchtbauer-Ladenburg formula. Figure 4(b) shows the temperature-dependent absorption cross sections and absorption coefficients.

Even using an Yb:KYF sample as thick as 14.3 mm, we were not able to reliably measure absorption coefficients below values of 10^{-2} cm^{-1}. To get access to the precise absorption in spectral regions with lower absorption coefficients, we calculated the absorption coefficients from the absorption cross sections derived using the reciprocity relation and the Yb^{3+} density ($n_{Yb} = 4.7 \cdot 10^{20}$ cm^3). In this way, we retrieved even two orders of magnitude lower absorption coefficients down to $\approx 10^{-4}$ cm^{-1}. The good agreement with the measured absorption coefficients for values above 10^{-2} cm^{-1} confirms the reliability of this method. Thus, the absorption

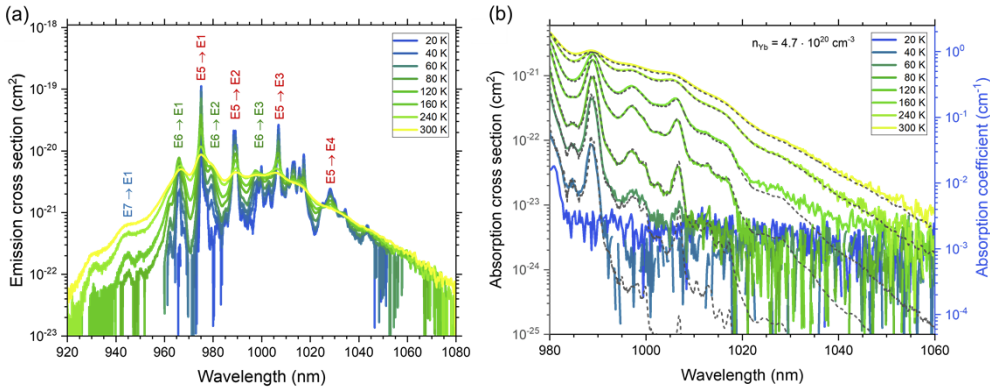

Fig. 4. (a) Emission cross section spectra of Yb:KYF at various temperatures. Resonant transitions between Stark levels are labeled. (b) Temperature-dependent absorption spectra of Yb:KYF for wavelengths longer than 980 nm. The colored lines were derived from the measured transmission spectra, and the black dashed lines were calculated from the emission cross section spectra using the reciprocity relation.

Optics EXPRESS

coefficients retrieved from the emission measurements were used for the calculations in the following Sections 4 and 5.

4. Laser cooling potential of Yb:KYF

The laser cooling efficiency by anti-Stokes fluorescence at a temperature T [42] is given as

$$\eta_c(\lambda,\ T) = \eta_{\text{ext}} \frac{\alpha_r(\lambda, T)}{\alpha_r(\lambda, T) + \alpha_b} \cdot \frac{\lambda_{\text{ex}}}{\lambda_f(T)} - 1, \tag{1}$$

where η_{ext} is the external quantum efficiency defined as a fraction of emitted photons escaping the medium with respect to the excited laser cooling ions, α_r is the resonant absorption coefficient by the laser cooling ions, α_b is the background absorption coefficient due to impurities, λ_{ex} is the excitation wavelength, and $\lambda_f(T)$ is the mean fluorescence wavelength defined by

$$\lambda_f(T) = \frac{\int[\lambda I_f(\lambda, T)]d\lambda}{\int I_f(\lambda, T)d\lambda}. \tag{2}$$

Here $I_f(\lambda,T)$ is the fluorescence intensity at a wavelength λ and a temperature T. From Eq. (1), one can immediately see that the excitation wavelength λ_{ex} has to be longer than the mean fluorescence wavelength λ_f to enable cooling, but with increasing excitation wavelength α_{r} decreases strongly [cf. Figure 4(b)] and the influence of background absorption becomes significant. Hence, there is an optimum wavelength maximizing η_{c}. Note that the fluorescence intensity spectrum I_f only considers emitted photons leaving the laser cooling medium. However, in Yb^{3+}-doped gain media, a part of the emitted fluorescence is reabsorbed. Thus, the measured mean fluorescence wavelength λ_f is red-shifted from the intrinsic value λ_{f0} calculated from the reabsorption-free fluorescence spectra. Consequently, the actual values of λ_f depend on the geometry of the cooling medium as well as of the excitation. Therefore, to discuss the intrinsic potential of Yb:KYF as a laser cooling medium, all the following calculations are based on λ_{f0}. Figure 5(a) shows the temperature dependence of the intrinsic mean fluorescence wavelength λ_{f0} for Yb:KYF. For comparison, the values for Yb:YLF [34] are also plotted.

For all Yb^{3+}-doped materials, the mean fluorescence wavelength undergoes a red-shift towards lower temperatures, as the transitions from the upper Stark levels E6 and E7 gradually vanish owing to their decreasing fractional occupancies as seen in Fig. 2(b). At all temperatures, the intrinsic mean fluorescence wavelength λ_{f0} of Yb:KYF is about 10 nm shorter than that of Yb:YLF, even though the barycenters of both lower and upper Stark manifolds differ only by $\approx$10 cm^{-1} between the two crystals [24]. This is because, as seen in Fig. 4(a), for Yb:KYF the highest energy emission transitions terminating at E1 are stronger than those terminating in the other lower Stark levels. In contrast, for Yb:YLF the strongest emission transitions are E5→E2 and E5→E3 [34]. The higher radiative decay rate from the level E6 than from E5, evidenced by their individual radiative lifetimes ($\tau_{\text{E5}} = 3.2$ ms, $\tau_{\text{E6}} = 1.1$ ms), also contributes to the shorter mean fluorescence wavelength compared with Yb:YLF.

To quantify the suitability of a given material for laser cooling based on its spectroscopic properties, we introduce a material figure-of-merit F_{cool}, extended from the one introduced by Bowman [43] to consider the dependency on the excitation wavelength and temperature, as follows:

$$F_{\text{cool}}(\lambda_{\text{ex}}, T) = \sigma_{\text{abs}}(\lambda_{\text{ex}}, T)\left(\frac{\lambda_{\text{ex}}}{\lambda_{f0}(T)} - 1\right). \tag{3}$$

F_{cool} is the product of the absorption cross section σ_{abs} and the laser cooling efficiency defined in Eq. (1) under the assumption of 100% external quantum efficiency and the absence of background absorption, as a function of the excitation wavelength λ_{ex}. To calculate F_{cool} as a material-specific

Optics EXPRESS

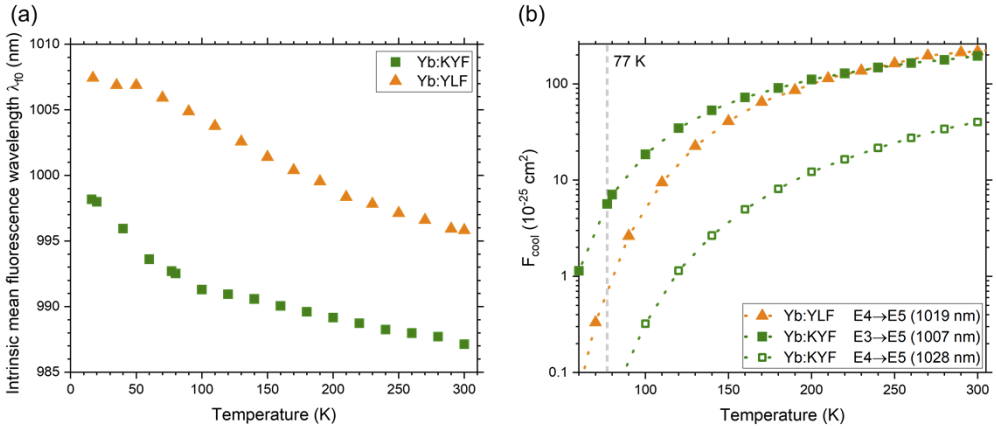

Fig. 5. (a) Intrinsic mean fluorescence wavelength of Yb:KYF and Yb:YLF versus temperature. The values for Yb:YLF are from [34]. (b) Material figure-of-merit for laser cooling F_{cool} of Yb:KYF for excitation transitions E3→E5 and E4→E5 compared with Yb:YLF (for π-polarized excitation) at the excitation wavelength indicated in brackets versus temperature. Note that the excitation transition E3→E4 will lead to negative values for Yb:YLF, as the corresponding excitation wavelength of 995.1 nm is shorter than the mean fluorescence wavelength at room temperature of 995.8 nm.

parameter, the intrinsic mean fluorescence wavelength λ_{f0} is used instead of the sample-specific λ_f. In the temperature range of 50–300 K, the maximum of F_{cool} is found at $\lambda_{\mathrm{ex}} = 1007$ nm for Yb:KYF and at $_{\mathrm{x}} = 1019$ nm for Yb:YLF, corresponding to the resonant transitions E3→E5 and E4→E5, respectively. Figure 5(b) shows the calculated temperature-dependent F_{cool} for Yb:KYF and Yb:YLF (for π-polarized excitation) in a logarithmic scale. The fractional occupancy of the level E4 in Yb:KYF is less than 5% even at room temperature and drops to below 1% at 180 K [cf. Figure 2(b)]. Thus, excitation at 1028 nm corresponding to the transition E4→E5 is not suited for cryogenic cooling because it yields significantly lower F_{cool} values. Instead, the level E3 can be regarded as a 'quasi-uppermost' level. Note that the wavelength corresponding to the transition E3→E5 is often shorter than the mean fluorescence wavelength in other materials, *e.g.*, in Yb:YLF. At room temperature, the maximum of F_{cool} is slightly higher for Yb:YLF than for Yb:KYF. However, for temperatures below 200 K the values for Yb:KYF exceed those of Yb:YLF. Note that the maximum is about five times higher for Yb:KYF than the value for Yb:YLF at the lowest temperature of 87 K achieved so far [18,19], and is even about eight times higher at the boiling point of LN of 77 K. Thus, Yb:KYF appears to be a promising material to achieve even lower temperatures than Yb:YLF.

5. LITMoS test: laser cooling characterization of Yb:KYF

F_{cool} indicates the general suitability of an idealized sample of a material to be cooled by anti-Stokes fluorescence. Nevertheless, the actual laser cooling performance of a given sample depends on the purity of the material. For laser cooling using rare-earth-doped solids, foreign rare-earth ions [44,45] and transition-metal ions [46,47] have been identified to be the main detrimental impurities. Foreign rare-earth ions can deexcite neighboring laser-cooling ions by energy transfer, which reduces the quantum efficiency and causes parasitic heating by non-radiative processes. Transition-metal ions have been considered the primary cause of background absorption [46]. In addition, oxides and hydroxides in fluoride crystals are also detrimental, because these impurities create high-energy phonon modes and cause multi-phonon relaxation [47]. The LITMoS test [12] is a useful method to reveal the quality of a specific laser cooling

Optics EXPRESS

medium. It is used to quantify the values of η_{ext} and α_{b} from Eq. (1) which are sample-specific and reduce the maximum cooling efficiency from its ideal cooling efficiency.

Due to the difficulties in the accurate determination of the actual mean fluorescence wavelength λ_f mentioned above we propose to instead use the intrinsic mean fluorescence wavelength λ_{f0} and to modify Eq. (1) as follows:

$$\eta_c^*(\lambda, T) = \eta_{\text{ext}} \frac{\alpha_r(\lambda, T)}{\alpha_r(\lambda, T) + \alpha_b} \cdot \frac{\lambda_{\text{ex}}}{\beta \lambda_{f0}(T)} - 1, . \tag{4}$$

where the coefficient $\beta = \lambda_f/\lambda_{f0}$ represents the relative red-shift of the actual mean fluorescence wavelength λ_f with respect to the intrinsic value λ_{f0}. As β is unknown, the LITMoS test thus yields the quantity η_{ext}/β instead of η_{ext}.

We performed LITMoS tests for our crystals to evaluate their sample-specific parameters η_{ext}/β and α_b. To this end, we prepared a cuboid-shaped sample from each of the two Yb:KYF and three Yb:YLF crystals. All six facets were polished to optical grade. The dimensions of the samples are summarized in Tab. 2. The crystallographic c-axis of the uniaxial Yb:YLF crystals was oriented perpendicular to the laser direction, yielding π-polarized excitation for all samples. A schematic of the LITMoS setup is shown in Fig. 6. The sample is placed on two optical glass fibers of 125 µm in diameter suspended over a copper block in a vacuum chamber to minimize the conductive heat from the supports. The chamber is evacuated to below 10^{-6} mbar by a turbo-molecular pump to reduce the convective heat exchange with the surroundings. A thin-disk laser based on Yb:$Lu_3Al_5O_{12}$ as the active medium is used as an excitation source. The laser is tunable between 990 nm and 1084 nm and excited the sample through an anti-reflection-coated glass window with a maximum incident power of 4 W at 1030 nm. The laser-induced temperature modulation ΔT was detected by a thermal camera (FLIR, SC645), and the power absorbed by the sample P_{abs} was determined using two thermal power meters (Ophir, 10A). In thermal equilibrium, we can assume the cooling efficiency η_{c} to be proportional to the induced temperature change per absorbed power $\Delta T \cdot {P_{\text{abs}}}^{-1}$. This proportionality was experimentally verified in our setup for ΔT up to, at least, ± 25 K around room temperature.

Both Yb:KYF samples showed cooling in the LITMoS tests. The maximum temperature decrease was 2.5 K at $\lambda_{\text{ex}} = 1016.9$ nm with an absorbed power of 470 mW for Yb:KYF-1 and 2.7 K at $\lambda_{\text{ex}} = 1018.2$ nm with an absorbed power of 230 mW for Yb:KYF-2. Figure 7(a) shows

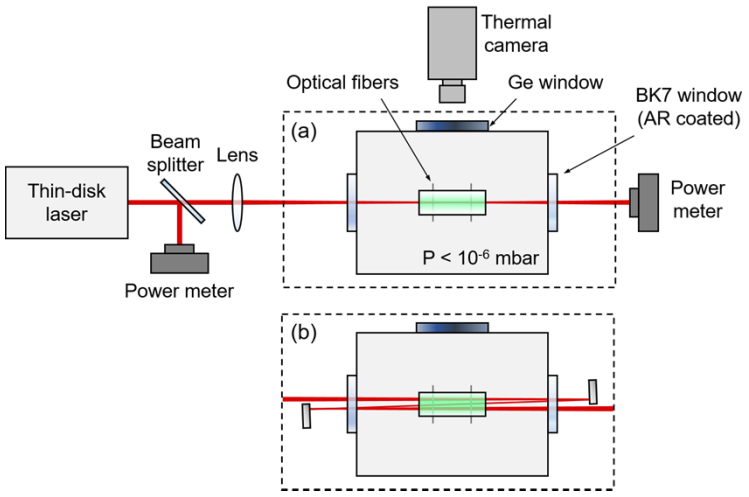

Fig. 6. Schematic of the LITMoS setup for (a) single-beam-pass and (b) triple-beam-pass configuration.

Optics EXPRESS

Table 2. LITMoS test results and calculated global MAT with corresponding excitation wavelength.

Crystal	Yb^{3+} density [10^{20} cm^{-3}]	Dimension [mm^3]	λ_{X1} [nm]	λ_{X2} [nm]	η_{ext}/β [%]	α_b [10^{-4} cm^{-1}]	global MAT [K] (λ_{ex})
Yb:KYF-1	4.7	5.8 5.8 14.3	1005.8	1058.3	98.1 ± 0.2	1.2 ± 0.3	149 (1017 nm)
Yb:KYF-2	4.7	4.7 4.6 13.7	1001.5	1066.5	98.6 ± 0.1	0.7 ± 0.3	105 (1013 nm)
Yb:YLF-1	6.5	4.1 4.0 13.8	1012.8	1036.4	98.4 ± 0.1	13.0 ± 0.3	169 (1019 nm)
Yb:YLF-2	6.5	3.8 2.9 11.8	1003.1	1065.7	99.3 ± 0.1	2.0 ± 0.3	100 (1019 nm)
Yb:YLF-3	6.4	4.6 3.9 15.1	1007.1	1069.0	98.9 ± 0.1	1.0 ± 0.3	99 (1019 nm)

$\Delta T \cdot P_{abs}{}^{-1}$ versus the excitation wavelength, hereafter simply named LITMoS result, for both Yb:KYF samples obtained in the single-beam-pass configuration shown in Fig. 6(a). Each LITMoS result exhibits two zero-crossing wavelengths λ_{X1} and λ_{X2} ($\lambda_{X1} < \lambda_{X2}$) at which neither heating nor cooling is observed. The shorter zero-crossing wavelength λ_{X1} is mainly influenced by η_{ext}/β, since the resonant absorption coefficient α_r in this wavelength range is by orders of magnitude higher than the background absorption coefficient α_b, thus $\alpha_r(\lambda_{X1})/[\alpha_r(\lambda_{X1}) + \alpha_b] \approx 1$ in Eq. (4). On the other hand, the longer zero-crossing wavelength λ_{X2} is sensitive to α_b, since the parasitic heating by impurities balances with the low cooling power due to low Yb^{3+} absorption at this wavelength. For the results shown in Fig. 7 (a), the least mean square fittings with Eq. (4) to the LITMoS results were not precise with respect to the parameter α_b. This is caused by the uncertainty in the precise determination of the longer zero-crossing wavelength λ_{X2} resulting from the small absorbed power P_{abs} and hence the small temperature change at long excitation wavelengths. To refine λ_{X2}, we thus modified the setup to the triple-beam-pass configuration shown in Fig. 6(b) to increase P_{abs} and ΔT. In this way, we determined the long-wavelength zero-crossing wavelengths λ_{X2} to be 1058.3 nm and 1066.5 nm for Yb:KYF-1 and Yb:KYF-2 and accordingly retrieved the background absorption coefficients to be $(1.2 \pm 0.3) \cdot 10^{-4}$ cm^{-1} and $(0.7 \pm 0.3) \cdot 10^{-4}$ cm^{-1}, respectively. The best-fitting results, shown as the blue solid lines in Fig. 7(a), correspond to the values of η_{ext}/β and α_b denoted in the figure.

Table 2 summarizes the LITMoS results for all five Yb:YLF and Yb:KYF samples. The sample-specific external quantum efficiency η_{ext}/β for Yb:KYF-2 is lower than for Yb:YLF-2,

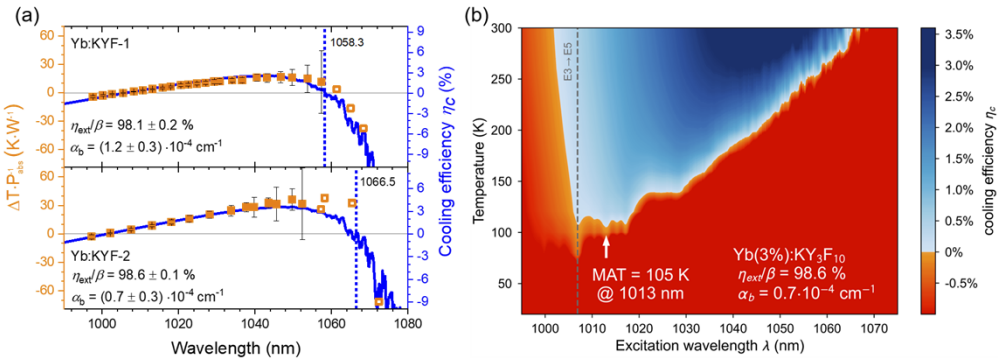

Fig. 7. (a) LITMoS test results of Yb:KYF-1 and Yb:KYF-2. The blue solid lines show the best fits using Eq. (1). (b) Temperature-dependent cooling efficiency of Yb:KYF-2 with an estimated global minimal achievable temperature (MAT) of 105 K at an excitation wavelength of 1013 nm. The excitation wavelength of 1007 nm maximizing F_{cool} for the ideal case is shown as the grey dashed vertical line corresponding to the transition E3→E5.

Optics EXPRESS

even though identical YF_3 and YbF_3 starting materials were used for these crystals. There are three explanations for this result:

I) The quantity β representing the amount of red-shift of mean fluorescence wavelength is different between Yb:YLF and Yb:KYF. We found that the overlap of absorption and emission spectra is larger for Yb:KYF than Yb:YLF. Thus, even though the size of the samples is comparable (see Tab. 2), reabsorption is stronger in Yb:KYF over the whole temperature range.

II) Energy transfer from Yb^{3+} to foreign rare-earth impurities, in particular Ho^{3+}, Er^{3+}, and Tm^{3+} [45], may be more pronounced in KYF than in YLF. This was experimentally confirmed for Tm^{3+} [48] and Dy^{3+} [22].

III) KYF may contain higher amounts of undesired oxides and/or OH^-, since KF, one of the raw materials of KYF, is strongly hygroscopic. Such impurities cause highly energetic phonon modes and thus promote non-radiative relaxation of Yb^{3+} [47].

All three factors must contribute to the laser cooling performance of Yb:KYF; however, further investigations are required to identify the most dominant one.

Despite using identical starting materials for Yb:YLF-1 and Yb:YLF-2, the background absorption coefficient α_b in Yb:YLF-1 is more than six times larger than in Yb:YLF-2. This can be due to transition-metal impurities introduced by the graphite crucible used for the growth of Yb:YLF-1 with the possible insufficient pre-cleaning process, as a platinum crucible pre-cleaned by HCl was used to grow Yb:YLF-2. The difference in the LITMoS results between Yb:YLF-2 and Yb:YLF-3 is attributed to the different LiF and YF_3 starting materials (see Tab. 1). Interestingly, the background absorption in Yb:KYF is lower than in Yb:YLF. Yb:KYF-1 exhibits a background absorption coefficient comparable with Yb:YLF-2 and -3, although the nominal purity of the used YF_3 is lower for Yb:KYF-1 (cf. Table 1). The background absorption α_b of Yb:KYF-2 below 10^{-4} cm^{-1} is among the lowest ever reported for Yb^{3+}-doped fluoride crystals. Even though further investigations on the reason for this observation are needed, our experimental results show the advantage of Yb:KYF to achieve lower background absorption compared with Yb:YLF.

For each sample, we calculated the cooling efficiency as a function of excitation wavelength and temperature using Eq. (4) based on the temperature-dependent spectroscopic data and the parameters η_{ext}/β and α_b listed in Tab. 2. Figure 7(b) shows the result for Yb:KYF-2 calculated with the sample-specific parameters denoted in the figure. This model calculation reveals minimum achievable temperatures (MATs), defined as the lowest temperature at which the cooling efficiency is still positive, at a given excitation wavelength λ_{ex}. The global MAT, the lowest MAT, of each sample with the corresponding excitation wavelength is also listed in Tab. 2. Note that this calculation does not consider the temperature dependency in η_{ext}/β and α_b. While the reabsorption eventually vanishes for Yb:YLF at lower temperatures [34], Yb:KYF still shows an overlap of its absorption and emission spectra even at 15 K [cf. Figure 1(b)] and thus reabsorption. Consequently, the temperature dependency in β is expected to be smaller in Yb:KYF than in Yb:YLF. Note that the background absorption α_b can also decrease by an order of magnitude in Yb:YLF when cooled from 300 K to 100 K [19]. Therefore, the actual MATs are expected to be lower than the calculated values. Nevertheless, this simplified estimation is still useful to discuss the potential of materials for all-solid-state optical cryocoolers.

From Tab. 2 it is evident that the calculated wavelengths required to reach the global MAT in Yb:KYF-1 and Yb:KYF-2 are longer than the excitation wavelength of 1007 nm at which F_{cool} is maximized. However, for Yb:KYF-2 even a minor increase of η_{ext}/β by only 0.2% shifts the optimum excitation wavelength from 1013 nm to 1007 nm with a reduced global MAT of 92 K. Such small changes may not even require improved crystal quality, but could *e.g.* be achieved by

Optics EXPRESS

reducing the crystal dimensions and thus β. In contrast, for all three Yb:YLF samples the global MAT was found at 1019 nm regardless of their η_{ext}/β and α_b, and the effect of improving η_{ext}/β was found to be much less pronounced.

6. Conclusion

We presented a detailed characterization of Yb:KYF and Yb:YLF crystals with respect to their potential for laser cooling by anti-Stokes fluorescence. For the first time, we experimentally demonstrate laser cooling in the cubic fluoride crystal Yb:KYF. Our temperature-dependent spectroscopic investigations revealed the cooling potential of Yb:KYF to be even higher than Yb:YLF at temperatures below 200 K. Even though the excitation transition from the uppermost ground-state Stark level E4 is known to be best-suited for cryogenic cooling in Yb:YLF, Yb:KYF shows its optimum excitation from the second-highest Stark level E3 owing to its mean fluorescence wavelength still shorter than the corresponding excitation wavelength. This feature allows the eight times larger maximum of figure-of-merit F_{cool} of Yb:KYF than Yb:YLF at the boiling point of LN. Therefore, Yb:KYF has the potential to reach temperatures lower than those achieved by the state-of-the-art material Yb:YLF (<87 K) [18,19]. The Czochralski-grown Yb(3%):KYF crystals yielded sample-specific values η_{ext}/β of up to 98.6% which are only slightly below the values observed in our Yb:YLF samples and partly caused by the larger red-shift of mean fluorescence wavelength β by reabsorption in Yb:KYF. Our growth and LITMoS results indicate that Yb:KYF exhibits lower background absorption than Yb:YLF even though a comparable amount of transition-metal impurities is expected in the raw materials. The obtained background absorption coefficient as low as $(0.7 \pm 0.3)\cdot 10^{-4}$ cm^{-1} is the lowest ever reported for Yb^{3+}-doped fluoride crystals. Note that imperfections of the grown Yb:KYF crystals attributed to the strong hygroscopicity of KF as well as the limited purity (4N) of the used KF powder leave room for further improvement. From the LITMoS test results of our Yb(3%):KYF and Yb(5%):YLF grown using the identical 5N YF_3 and YbF_3 starting materials (Yb:KYF-2 and Yb:YLF-2), we estimated their global MATs to be ≈100 K for both samples. Even a minor increase in η_{ext}/β, *e.g.*, by improving the sample geometry to mitigate reabsorption, can significantly reduce the global MAT of Yb:KYF. We thus conclude that Yb:KYF crystals have the potential to exceed Yb:YLF in regards to laser cooling and to be used in all-solid-state optical cryocoolers to replace LN cryostats in various applications.

Acknowledgments. The authors thank Celine Kapella for the technical support for the growth of the fluoride crystals, Michael Schulze for support with determining doping concentrations by X-ray fluorescence, Albert Kwasniewski for orienting the Yb:YLF crystals by X-ray diffraction, and Katrin Berger, Manuela Imming-Friedland, and Thomas Wurche for the sample preparation.

Disclosures. The authors declare no conflicts of interest.

Data availability. The data that support the results presented in this article are available from the authors upon request.

References

1. M. Sheik-Bahae and R. I. Epstein, "Laser cooling of solids," Laser Photonics Rev. **3**(1-2), 67–84 (2009).
2. D. V. Seletskiy, R. Epstein, and M. Sheik-Bahae, "Laser cooling in solids: Advances and prospects," Rep. Prog. Phys. **79**(9), 096401 (2016).
3. M. P. Hehlen, J. Meng, A. R. Albrecht, E. R. Lee, A. Gragossian, S. P. Love, C. E. Hamilton, R. I. Epstein, and M. Sheik-Bahae, "First demonstration of an all-solid-state optical cryocooler," Light: Sci. Appl. **7**, 15 (2018).
4. D. L. Upp, R. M. Keyser, and T. R. Twomey, "New cooling methods for HPGE detectors and associated electronics," J. Radioanal. Nucl. Chem. **264**(1), 121–126 (2005).
5. R. Vicente, G. Nogues, J.-M. Niot, T. Wiertz, P. Contini, and A. Gardelein, "Impacts of laser cooling for low earth orbit observation satellites: An analysis in terms of size, weight and power," Cryogenics **105**, 103000 (2020).
6. P. Pringsheim, "Zwei Bemerkungen über den Unterschied von Lumineszenz- und Temperaturstrahlung," Z. Physik **57**(11-12), 739–746 (1929).
7. R. I. Epstein, M. I. Buchwald, B. C. Edwards, T. R. Gosnell, and C. E. Mungan, "Observation of laser-induced fluorescent cooling of a solid," Nature **377**(6549), 500–503 (1995).

Optics EXPRESS

8. Y. Lei, B. Zhong, T. Yang, X. Duan, M. Xia, C. Wang, J. Xu, Z. Zhang, J. Ding, and J. Yin, "Laser cooling of Yb^{3+}:$LuLiF_4$ crystal below cryogenic temperature to 121 K," Appl. Phys. Lett. **120**(23), 231101 (2022).
9. S. D. Melgaard, A. R. Albrecht, M. P. Hehlen, and M. Sheik-Bahae, "Solid-state optical refrigeration to sub-100 Kelvin regime," Sci. Rep. **6**(1), 20380 (2016).
10. R. Vicente, G. Cittadino, A. Di Lieto, M. Tonelli, A. Gardelein, and G. Nogues, "Operation of a fiber-coupled laser-cooler down to cryogenic temperatures," Opt. Express **30**(8), 12929–12936 (2022).
11. J. L. Kock, A. R. Albrecht, R. I. Epstein, and M. Sheik-Bahae, "Optical refrigeration of payloads to T< 125 K," Opt. Lett. **47**(18), 4720–4723 (2022).
12. S. Melgaard, *Cryogenic optical refrigeration: Laser cooling of solids below 123 K*, (University of New Mexico, 2013).
13. A. Volpi, K. W. Krämer, D. Biner, B. Wiggins, J. Kock, A. R. Albrecht, E. J. Peterson, M. N. Spilde, M. Sheik-Bahae, and M. P. Hehlen, "Bridgman Growth of Laser-Cooling-Grade $LiLuF_4$:Yb^{3+} Single Crystals," Cryst. Growth Des. **21**(4), 2142–2153 (2021).
14. A. Volpi, G. Cittadino, A. Di Lieto, and M. Tonelli, "Anti-Stokes cooling of Yb-doped KYF_4 single crystals," J. Lumin. **203**, 670–675 (2018).
15. S. Püschel, F. Mauerhoff, C. Kränkel, and H. Tanaka, "Solid-state laser cooling in Yb:CaF_2 and Yb:SrF_2 by anti-Stokes fluorescence," Opt. Lett. **47**(2), 333–336 (2022).
16. S. Rostami, A. R. Albrecht, A. Volpi, M. P. Hehlen, M. Tonelli, and M. Sheik-Bahae, "Tm-doped crystals for mid-IR optical cryocoolers and radiation balanced lasers," Opt. Lett. **44**(6), 1419–1422 (2019).
17. S. Bigotta, D. Parisi, L. Bonelli, A. Toncelli, M. Tonelli, and A. Di Lieto, "Spectroscopic and laser cooling results on Yb^{3+}-doped BaY_2F_8 single crystal," J. Appl. Phys. **100**(1), 013109 (2006).
18. A. Gragossian, M. Ghasemkhani, J. Meng, A. Albrecht, M. Tonelli, and M. Sheik-Bahae, "Optical refrigeration inches toward liquid-nitrogen temperatures," *SPIE Newsroom* (2017).
19. A. Volpi, J. Meng, A. Gragossian, A. R. Albrecht, S. Rostami, A. D. Lieto, R. I. Epstein, M. Tonelli, M. P. Hehlen, and M. Sheik-Bahae, "Optical refrigeration: the role of parasitic absorption at cryogenic temperatures," Opt. Express **27**(21), 29710–29718 (2019).
20. H. Guggenheim, "Growth of highly perfect fluoride single crystals for optical masers," J. Appl. Phys. **34**(8), 2482–2485 (1963).
21. D. Maier, R. Bertram, D. Klimm, and R. Fornari, "Influence of the atmosphere on the growth of $LiYF_4$ single crystal fibers by the micro-pulling-down method," Cryst. Res. Technol. **44**(2), 137–140 (2009).
22. P. P. Fedorov, V. V. Semashko, and S. L. Korableva, "Lithium Rare-Earth Fluorides As Photonic Materials: 1. Physicochemical Characterization," Inorg. Mater. **58**(3), 223–245 (2022).
23. R. E. Thoma, C. F. Weaver, H. A. Friedman, H. Insley, L. A. Harris, and H. A. Yakel, "Phase equilibria in the system LiF-YF_3," J. Phys. Chem. **65**(7), 1096–1099 (1961).
24. M. Ito, G. Boulon, A. Bensalah, Y. Guyot, C. Goutaudier, and H. Sato, "Spectroscopic properties, concentration quenching, and prediction of infrared laser emission of Yb^{3+}-doped KY_3F_{10} cubic crystal," J. Opt. Soc. Am. B **24**(12), 3023–3033 (2007).
25. P. Camy, J.-L. Doualan, R. Moncorgé, J. Bengoechea, and U. Weichmann, "Diode-pumped Pr^{3+}:KY_3F_{10} red laser," Opt. Lett. **32**(11), 1462–1464 (2007).
26. M. A. Dubinskii, "New fluoride laser hosts with natural site for rare-earth and actinide activation," in *Advanced Solid State Lasers* (OSA, 1991), p. MT2.
27. M. A. Dubinskii, K. L. Schepler, A. K. Naumov, V. V. Semashko, R. Y. Abdulsabirov, and S. L. Korableva, "New CW low-threshold laser for diode pumping based on Nd3+:KY3F10," in *Advanced Solid State Lasers* (OSA, 1997), p. CW4.
28. A. Braud, P. Y. Tigreat, J. L. Doualan, and R. Moncorgé, "Spectroscopy and cw operation of a 1.85 µm Tm:KY_3F_{10} laser," Appl. Phys. B **72**(8), 909–912 (2001).
29. A. Grzechnik, J. Nuss, K. Friese, J.-Y. Gesland, and M. Jansen, "Refinement of the crystal structure of potassium triyttrium decafluoride, KY_3F_{10}," Z. Kristallogr. - New Cryst. Struct. **217**(JG), 460 (2002).
30. P. W. Metz, T. Calmano, D.-T. Marzahl, C. Kränkel, and G. Huber, "Polarization effects in Pr^{3+}-doped cubic KY_3F_{10} and stable dual wavelength lasing," in *Advanced Solid State Lasers* (OSA, 2015), p. ATu1A.3.
31. M. Mortier, J. Y. Gesland, M. Rousseau, M. A. Pimenta, L. O. Ladeira, J. C. M. Da Silva, and G. A. Barbosa, "Raman scattering investigations of KY_3F_{10}," J. Raman Spectrosc. **22**(7), 393–396 (1991).
32. F.-X. Gan and H.-Y. Chen, "Raman spectra of $LiYF_4$ crystal," Chinese Phys. Lett. **2**(9), 421–424 (1985).
33. M. P. Hehlen, "Novel materials for laser refrigeration," in *Laser Refrigeration of Solids II*, 7228R. I. Epstein and M. Sheik-Bahae, eds. (2009), Vol. 7228, p. 72280E.
34. S. Püschel, S. Kalusniak, C. Kränkel, and H. Tanaka, "Temperature-dependent radiative lifetime of Yb:YLF: refined cross sections and potential for laser cooling," Opt. Express **29**(7), 11106–11120 (2021).
35. B. Aull and H. Jenssen, "Vibronic interactions in Nd:YAG resulting in nonreciprocity of absorption and stimulated emission cross sections," IEEE J. Quantum Electron. **18**(5), 925–930 (1982).
36. D. E. McCumber, "Einstein Relations Connecting Broadband Emission and Absorption Spectra," Phys. Rev. **136**(4A), A954–A957 (1964).
37. W.-L. Feng and W.-C. Zheng, "Theoretical calculations of the optical band positions and spin-Hamiltonian parameters for Yb^{3+} at the tetragonal Y^{3+} site of KY_3F_{10} crystal," Phys. B **406**(13), 2580–2582 (2011).

Optics EXPRESS

38. H. Kühn, S. T. Fredrich-Thornton, C. Kränkel, R. Peters, and K. Petermann, "Model for the calculation of radiation trapping and description of the pinhole method," Opt. Lett. **32**(13), 1908–1910 (2007).
39. P. Y. Tigreat, J. L. Doualan, C. Budasca, and R. Moncorge, "Energy transfer processes in (Yb^{3+}, Dy^{3+}) and (Tm^{3+}, Dy^{3+}) codoped $LiYF_4$ and KY_3F_{10} single crystals," J. Lumin. **94-95**, 23–27 (2001).
40. L. D. DeLoach, S. A. Payne, L. L. Chase, L. K. Smith, W. L. Kway, and W. F. Krupke, "Evaluation of Absorption and Emission Properties of Yb^{3+} Doped Crystals for Laser Applications," IEEE J. Quantum Electron. **29**(4), 1179–1191 (1993).
41. L. Bonelli, A. Toncelli, A. Di Lieto, and M. Tonelli, "Spectroscopic analysis of 10% Yb^{3+}:KYF_4 crystal," J. Phys. Chem. Solids **68**(12), 2381–2386 (2007).
42. C. W. Hoyt, M. P. Hasselbeck, M. Sheik-Bahae, R. I. Epstein, S. Greenfield, J. Thiede, J. Distel, and J. Valencia, "Advances in laser cooling of thulium-doped glass," J. Opt. Soc. Am. B **20**(5), 1066 (2003).
43. S. R. Bowman and C. E. Mungan, "New materials for optical cooling," Appl. Phys. B **71**(6), 807–811 (2000).
44. U. Demirbas, J. Thesinga, M. Kellert, M. Pergament, and F. X. Kärtner, "Temperature and doping dependence of fluorescence lifetime in Yb:YLF (role of impurities)," Opt. Mater. **112**, 110792 (2021).
45. A. Di Lieto, A. Sottile, A. Volpi, Z. Zhang, D. V. Seletskiy, and M. Tonelli, "Influence of other rare earth ions on the optical refrigeration efficiency in Yb:YLF crystals," Opt. Express **22**(23), 28572–28583 (2014).
46. S. Melgaard, D. Seletskiy, V. Polyak, Y. Asmerom, and M. Sheik-Bahae, "Identification of parasitic losses in Yb:YLF and prospects for optical refrigeration down to 80 K," Opt. Express **22**(7), 7756–7764 (2014).
47. M. P. Hehlen, R. I. Epstein, and H. Inoue, "Model of laser cooling in the Yb^{3+}-doped fluorozirconate glass ZBLAN," Phys. Rev. B **75**(14), 144302 (2007).
48. A. Braud, S. Girard, J. L. Doualan, M. Thuau, R. Moncorgé, and A. M. Tkachuk, "Energy-transfer processes in Yb:Tm-doped KY_3F_{10}, $LiYF_4$,and BaY_2F_8 single crystals for laser operation at 1.5 and 2.3 μm," Phys. Rev. B **61**(8), 5280–5292 (2000).